Optical Properties Characterization of TiO₂–Metakaolin Composites Synthesized by the Sol-Gel Method

Berlian Sitorus [1,*], Felicia Silaban [1], Anthoni B. Aritonang [1]

[1] Department of Chemistry, Faculty of Mathematics and Natural Sciences, Universitas Tanjungpura, Pontianak, West Kalimantan, Indonesia

* Corresponding author: berlian.sitorus@chemistry.untan.ac.id

Article Info

Abstract

Titanium dioxide (TiO_2) is a semiconductor known for its excellent optical properties and is widely used in various applications. In this study, TiO_2-Metakaolin composites were synthesized to investigate the optical properties of TiO_2-Metakaolin in comparison to pure TiO_2. The synthesis was conducted using the sol-gel method, with metakaolin concentrations varied at 0.5%, 1%, and 1.5% (w/v), based on the volume of the $Ti(OH)_n$ sol. XRF analysis revealed that the composite primarily consists of SiO_2, TiO_2, and Al_2O_3. XRD results confirmed that the synthesized TiO_2 is in the anatase phase, while kaolin transformed from crystalline to amorphous metakaolin. FTIR analysis identified absorption peaks at wave numbers $3410-3448$ cm^{-1} (OH), $2364-2357$ cm^{-1} (OH), $1624-1633$ cm^{-1} (Ti-OH), $1070-1072$ cm^{-1} (Si-O-Si), $800-823$ cm^{-1} (Ti-O), $547-555$ cm^{-1} (Si-O or Al-O), and $464-480$ cm^{-1} (Ti-O-Ti), indicating interactions between TiO_2 and metakaolin. DRS-UV characterization showed that the band gap energies of the TiO_2-metakaolin composites with metakaolin concentrations of 0.5%, 1%, and 1.5% (w/v) were 3.06 eV, 3.05 eV, and 3.11 eV, respectively. These values are lower than the band gap energy of pure TiO_2 (3.18 eV), demonstrating that metakaolin effectively reduces the band gap energy of TiO_2.

1. Introduction

Titanium dioxide (TiO_2) is a semiconductor material known for its excellent optical properties [1] and relatively inert nature compared to other compounds. It is non-toxic, exhibits high oxidation capability, and is cost-effective [2]. TiO_2 has a band gap energy ranging from 3.0 to 3.2 eV, which limits its active functionality to the UV light region [3]. To enhance its performance in the visible light spectrum, TiO_2 is often modified, typically by compositing it with other metals. However, this approach poses environmental concerns due to the generation of metal waste.

Another promising approach is the use of kaolin. Kaolin, primarily composed of SiO_2 and Al_2O_3, can enhance light scattering, thereby improving light absorption in the visible light region and suppressing electron recombination events [4]. When composited with TiO_2, kaolin can further increase absorption capacity due to its large porous structure [5]. Additionally, incorporating metakaolin in specific compositions has effectively reduced the band gap energy of TiO_2 [1].

Therefore, this study utilizes kaolin, which primarily consists of SiO_2 (46.54%) and Al_2O_3 (39.5%) [6]. Kaolin is then converted into its metastable form, metakaolin, which exhibits greater reactivity than kaolin [7]. The incorporation of metakaolin is achieved through the sol-gel method. This method is chosen due to its relatively simple equipment requirements, ability to produce uniform particle sizes, and capacity to yield high-purity materials [8].

This study synthesized TiO_2-metakaolin composites with metakaolin concentrations varied at 0.5%, 1%, and 1.5% (w/v), using the volume of $Ti(OH)_n$ sol as the base. The influence of metakaolin on the optical properties of TiO_2-metakaolin was investigated through characterization techniques, including X-ray fluorescence (XRF), X-ray diffraction (XRD), Fourier

Transform Infrared Spectroscopy (FTIR), and Diffuse Reflectance Spectroscopy (DRS) UV-Vis analysis.

2. Experimental

2.1. Materials

The tools utilized in this study included laboratory glassware, a reflux apparatus, a Shimadzu IR Prestige-21 Fourier Transform Infrared (FTIR) spectrophotometer, a Shimadzu UV-2450 DRS UV spectrophotometer, a furnace, an X-ray Diffraction (XRD) Philips X-ray instrument (40 kV), and an X-ray Fluorescence (XRF) PANalytical Epsilon 3 analyzer. The materials employed were distilled water, acetic acid (Merck), hydrochloric acid (Merck), acetylacetone (Merck), ethanol (Smart Lab), Capkala kaolin, and titanium tetraisopropoxide (Sigma Aldrich).

2.2. Synthesis of $Ti(OH)_n$ Sol

Solution A was prepared by mixing 2 mL of acetic acid and 2 mL of distilled water into 26.5 mL of ethanol. Solution B was made by dissolving 7.5 mL of titanium tetraisopropoxide (TTiP) in 26.5 mL of ethanol, which was then transferred into a reflux flask, stirred using a magnetic stirrer, and supplemented with 1 mL of acetylacetone. Solution A was slowly dripped into Solution B within the reflux apparatus at 55°C for 2 hours. The resulting solution was allowed to rest for 10 minutes until $Ti(OH)_n$ sol was formed [5].

2.3. Metakaolin Preparation

The preparation of Capkala kaolin involved washing the kaolin with distilled water until the pH of the wash water matched that of distilled water. The kaolin was then dried at 105°C for 5 hours. After drying, the kaolin was ground and sieved through a 150-mesh sieve to ensure uniform particle size. The processed kaolin was weighed and mixed with 2 M HCl in a 1:10 ratio, followed by stirring with a magnetic stirrer for 2 hours. The kaolin was then filtered and washed with distilled water until the pH of the kaolin matched that of distilled water. Subsequently, the kaolin was dried at 100°C for 3 hours [9]. Following this, the kaolin underwent physical activation by calcination at 700°C for 30 minutes. The calcined kaolin was then ground using a mortar at room temperature [6].

2.4. Synthesis of TiO_2-Metakaolin

The composite synthesis was done by rapidly stirring a specific amount of metakaolin while slowly adding $Ti(OH)_n$ sol. The metakaolin concentrations used were 0.5%, 1%, and 1.5% (w/v) relative to the volume of $Ti(OH)_n$ sol. The mixture was stirred continuously using a magnetic stirrer for 4 hours, followed by an aging process for 16 hours until the mixture formed a gel. The gel was then dried in an oven at 80°C for 3 hours and subsequently calcined at 450°C for 3 hours to obtain TiO_2-metakaolin composite crystals [10].

2.5. Characterization

The synthesized composites were characterized using XRF, XRD, FTIR, and DRS UV-Vis techniques. XRF analysis was performed to identify the elemental components present in the synthesized materials. XRD analysis was conducted to determine the phases and crystalline structures within the synthesis products. FTIR analysis was carried out to identify the functional groups present in each synthesized sample. DRS UV-Vis analysis was used to obtain reflectance, absorbance, and band gap energy data for pure TiO_2 and TiO_2-Metakaolin composites.

3. Results and Discussion

3.1. Synthesis of TiO_2 from TTiP

The synthesis of TiO_2 was carried out using TTiP as the precursor and ethanol as the solvent. Acetic acid served as the catalyst, while distilled water facilitated the hydrolysis reaction. Acetylacetone was added as a chelating agent to prevent agglomeration [11]. This process yielded $Ti(OH)_n$ sol, which underwent an aging process to form a more rigid gel. During aging, TTiP molecules polymerized, creating cross-linked chains that trapped the solvent within the structure. Subsequently, calcination was performed to thermally break the Ti-O bonds, allowing the formation of Ti-O-Ti bonds as the temperature decreased [12]. The final product of the synthesis was a white TiO_2 powder.

The synthesized products were subsequently analyzed using XRF testing to determine their chemical composition. Table 1 presents the composition of various oxide compounds identified in the synthesis results. The XRF results indicate that TiO_2 constitutes the highest proportion, confirming the high purity of the synthesized TiO_2. In addition to TiO_2, several other oxide compounds were detected, albeit in minor percentages.

Table 1. Composition of several oxide compounds of the synthesized product

Component	% Relative weight
TiO_2	96.5
P_2O_5	1.9
SiO_2	0.8
CaO	0.64
OsO_4	0.1
CuO	0.085
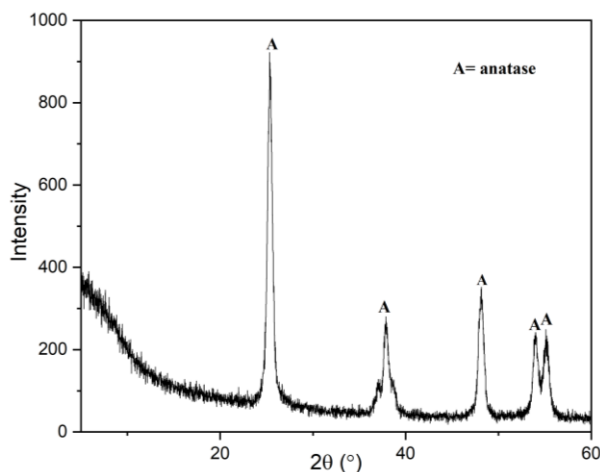
Figure 1. The diffractogram of synthesized material of TiO_2 with TTiP precursor

XRD is a technique used to determine the crystal structure and size of materials. Figure 1 displays the XRD pattern of TiO_2 synthesized using TTiP as the precursor. The XRD pattern of TiO_2 exhibits distinct peaks at 2θ values of 25.4°, 37.8°, 48.2°, 54°, and 55.2°. These peaks align with the anatase phase of TiO_2, as referenced in the International Center for Diffraction Data (ICDD) No. 98-004-4882 [13]. The crystallite size was calculated using the Debye-Scherrer equation (Equation 1).

$$D = \frac{K\lambda}{\beta cos\theta} \tag{1}$$

where D represents the crystal size, K is the shape factor of the crystal, λ is the wavelength of the X-rays, β is the Full Width at Half Maximum (FWHM), and θ is the diffraction angle. Using the Debye-Scherrer equation, the calculated crystal size of the synthesized TiO_2 is 19.5 nm.

3.2. Metakaolin Formation

Metakaolin is formed by changing kaolin into metakaolin through the dehydroxylation process. The dehydroxylation process aims to release the H_2O bonds in the kaolin structure [14]. Dehydroxylation results in the transformation of the kaolinite structure from crystalline to amorphous. The reactions are presented in Equation (2) [15].

$$Al_2Si_2O_5(OH)_4 \xrightarrow{700°C} Al_2Si_2O_7 + 2H_2O \tag{2}$$

Based on the XRF analysis results, the oxide content of kaolin and metakaolin is presented in Table 2. The analysis indicates that SiO_2 and Al_2O_3 are the dominant components in both kaolin and metakaolin, consistent with previous research showing that metakaolin primarily consists of SiO_2 and Al_2O_3 [16]. The XRD analysis results for the initial kaolin and after the dehydroxylation process at 700°C are shown in Figure 2.

Figure 2 shows the absence of a kaolinite peak and a decrease in peak intensity in the metakaolin diffractogram. This reduction in kaolinite is due to the transformation of the kaolinite crystal structure into an amorphous structure in metakaolin [17]. The decrease in kaolinite peak intensity is observed in the metakaolin diffractogram at 2θ = 19.7° (ICDD 00-003-0052). Compared to the kaolinite peak in kaolin at 2θ = 20° (ICDD 00-003-0059), the kaolinite peak in metakaolin exhibits lower intensity.

Table 2. The composition of the oxide content of kaolin and metakaolin

Kaolin		Metakaolin	
Component	% Relative weight	Component	% Relative weight
SiO_2	61	SiO_2	59
Al_2O_3	31.7	Al_2O_3	26.9
P_2O_5	3.3	P_2O_5	3.3
K_2O	2.9	K_2O	2.3
TiO_2	2.7	TiO_2	2.8
Fe_2O_3	2.8	Fe_2O_3	2.1
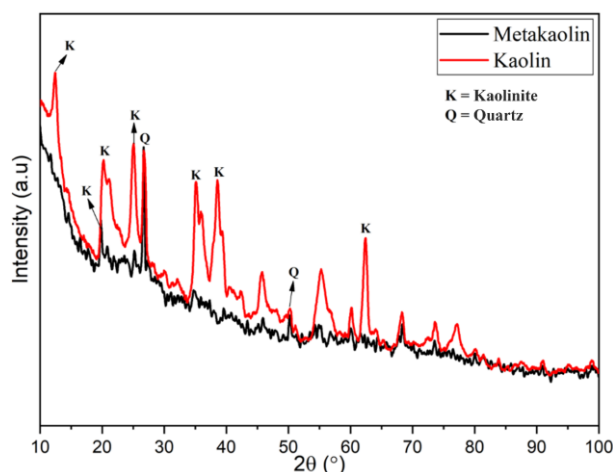
Figure 2. XRD analysis results of kaolin and metakaolin after the dehydroxylation process at 700°C

Kaolin undergoes a structural transformation from a diffractogram with sharp peaks to metakaolin, which exhibits broader, less distinct peaks. Sharp peaks indicate that kaolin is crystalline due to its well-defined atomic arrangement [18]. In contrast, the broad and diffuse peaks in the metakaolin diffractogram confirm its amorphous nature, characterized by an irregular atomic arrangement. The structural differences between kaolin and metakaolin influence the sharpness of the kaolinite peak and the broadening of the metakaolin peak [19]. This transformation is evident at angles 2θ = 12.5°, 20°, 25°, 35.1°, 38.6°, and 62.4°, which are characteristic of kaolinite minerals (ICDD 00-003-0059). However, these absorption peaks are not distinctly defined in the metakaolin diffractogram.

The crystal size of kaolin and metakaolin was determined using the Debye-Scherrer equation. The calculations indicate that the crystal size of kaolin is 36.9 nm, while that of metakaolin is 28 nm. The smaller crystal size of metakaolin is attributed to the broadening of its diffraction peak, as the Debye-Scherrer equation states that crystal size is inversely proportional to peak width (FWHM) [20].

3.3. Synthesis of TiO_2-Metakaolin

The synthesis of TiO_2-metakaolin was conducted using the sol-gel method, following the TiO_2 synthesis procedure. Metakaolin was added at varying concentrations of 0.5%, 1%, and 1.5% (w/v). XRF analysis was performed to determine the composition of TiO_2-metakaolin, as presented in Table 3.

Table 3. Oxide composition of TiO_2-metakaolin composites with varying metakaolin concentrations

Material	Relative weight percentage of oxides (%)		
	SiO_2	TiO_2	Al_2O_3
Metakaolin	59	2.8	26.9
TiO_2-Metakaolin 0.5%	29.2	44.2	17.6
TiO_2-Metakaolin 1%	31.2	40.9	13.4
TiO_2-Metakaolin 1.5%	39.2	30.6	21.7
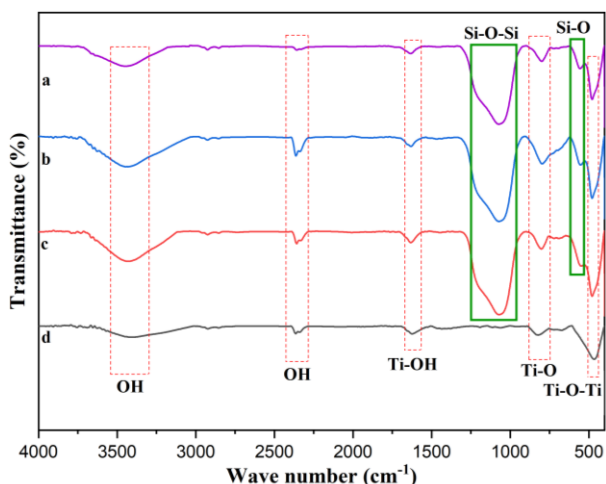
Figure 3. FTIR spectra of (a) TiO_2-Metakaolin 1.5% (w/v), (b) TiO_2-Metakaolin 1% (w/v), (c) TiO_2-Metakaolin 0.5% (w/v), and (d) TiO_2
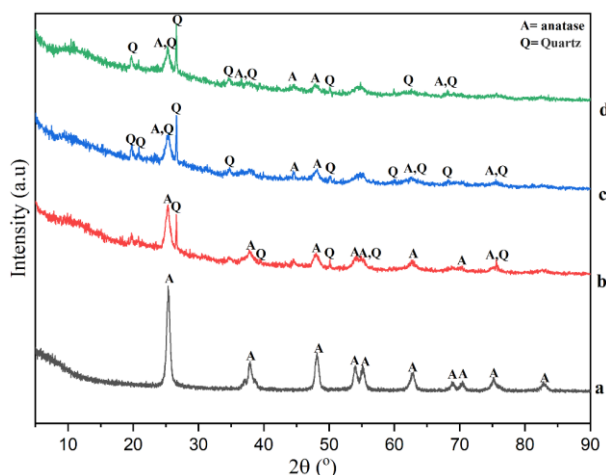
Figure 4. Diffractograms of (a) TiO_2, (b) TiO_2-Metakaolin 0.5% (w/v), (c) TiO_2-Metakaolin 1% (w/v), (d) TiO_2-Metakaolin 1.5% (w/v)

Table 3 shows that the obtained composites have similar main compositions. The TiO_2 content in the synthesized composites is higher than in the initial metakaolin. As the concentration of metakaolin increases, the SiO_2 content in the composite also increases due to the higher amount of added metakaolin.

Functional group analysis was performed to identify the functional groups in the TiO_2-metakaolin composite. The FTIR analysis results, shown in Figure 3, indicate the formation of new peaks in the spectra following the addition of metakaolin. The appearance of these new peaks suggests the occurrence of chemical interactions [21]. An absorption band is observed in the wavenumber range of 1070−1072 cm⁻¹, corresponding to the asymmetric stretching vibrations of Si−O−Si [22] originating from the SiO_2 in metakaolin. Additionally, a new absorption peak appears in the TiO_2 wavenumber range of 400−611 cm⁻¹, specifically between 547 and 555 cm⁻¹. This peak is attributed to the bending vibrations of Si−O or Al−O bonds derived from metakaolin [23].

The XRD analysis of TiO_2-metakaolin reveals a diffraction pattern characteristic of TiO_2 in the anatase phase (ICDD No. 01-073-1764) and SiO_2 in the quartz phase (ICDD No. 01-085-0798). This is evident from distinct peaks in each TiO_2-metakaolin variation, observed at 2θ = 25−26° and 48−50°. Combining these peaks within a single diffraction pattern confirms the successful synthesis of the material [24]. Variations in metakaolin concentration influence peak intensity, with increasing metakaolin content leading to a decrease in TiO_2 peak intensity [25]. As the concentration of metakaolin increases, the quartz phase becomes more dominant in the TiO_2-metakaolin composite. The crystal size of the synthesized TiO_2-metakaolin is 40.2 nm for 0.5% (w/v) TiO_2-metakaolin, 42 nm for 1% (w/v) TiO_2-metakaolin, and 26.4 nm for 1.5% (w/v) TiO_2-metakaolin. The addition of metakaolin reduces crystal size, as it inhibits the growth of TiO_2-metakaolin crystals [26].

3.4. Optical Properties

The absorbance spectra from the DRS UV-Vis analysis of the TiO_2-metakaolin composite are presented in Figure 5. The TiO_2-metakaolin composites exhibit different absorption characteristics compared to pure TiO_2. While TiO_2 shows high absorption in the UV region, its absorption capacity in the visible light region is very low, with most radiation being reflected. In contrast, TiO_2-metakaolin demonstrates a high absorption capacity in both the UV and visible light regions. Among the composites, TiO_2-metakaolin 0.5% exhibits the highest absorption capacity compared to TiO_2-metakaolin 1% and 1.5%. This trend aligns with the principle that lower reflectance corresponds to higher absorbance capacity, as reflectance is inversely proportional to absorbance [27].

The band gap energy was determined using the Tauc plot method with the Kubelka-Munk approach, as described in Equation (3) [28].

$$F(R) = \frac{(1-R)^2}{2R} = \frac{k}{s} \tag{3}$$

where $F(R)$ is the Kubelka Munk function, k is the absorption coefficient, s is the scattering factor, and R is the reflectance. The band gap energy (E_g) is obtained by plotting $[F(R)h\upsilon]^n$ against E_g where TiO_2 exhibits an indirect transition, making $n = \frac{1}{2}$. The band gap energy values are shown in Table 4.

Table 4. Band gap energy values and corresponding wavelengths of TiO_2 and TiO_2-metakaolin variations, calculated using the Kubelka-Munk method

Material	Wavelength (nm)	Band gap energy (eV)
TiO_2	390	3.18
TiO_2-Metakaolin 0.5%	405	3.06
TiO_2-Metakaolin 1%	407	3.05
TiO_2-Metakaolin 1.5%	399	3.11
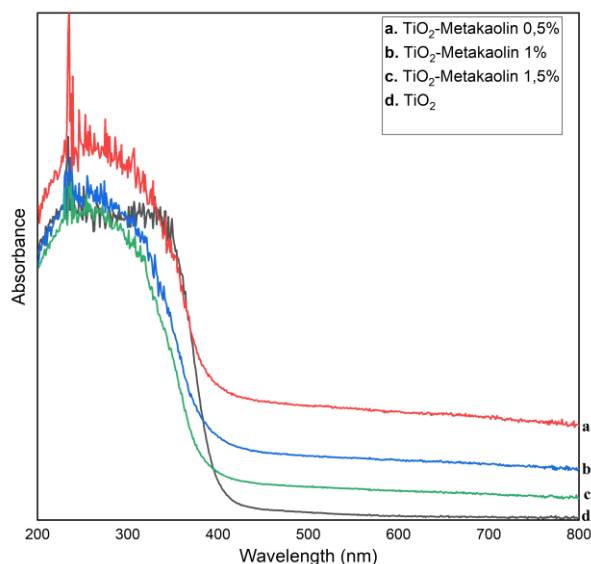
Figure 5. DRS spectra of TiO_2 and TiO_2-metakaolin with variations of 0.5%, 1%, and 1.5% (w/v) in the wavelength range of 200−800 nm

Table 4 shows that the synthesized TiO_2 has a band gap energy of 3.18 eV, corresponding to a wavelength of 390 nm. This confirms that the anatase phase of TiO_2 is active in the UV region. The addition of metakaolin to TiO_2 decreases its band gap energy, with 0.5% (w/v) metakaolin reducing it to 3.06 eV (405 nm), 1% to 3.05 eV (407 nm), and 1.5% to 3.11 eV (399 nm). This indicates that the TiO_2-metakaolin composite exhibits potential activity in the visible light region (380−780 nm) [29].

The lowest band gap energy was observed with the addition of 0.5% (w/v) metakaolin. The reduction in band gap energy upon metakaolin incorporation is attributed to the presence of impurities in TiO_2, which lead to the formation of new energy levels between the valence and conduction bands, thereby altering the band gap [30]. Additionally, the presence of SiO_2 and Al_2O_3 in metakaolin can influence electron recombination. However, excessive metakaolin content may hinder electron mobility [1]. These findings suggest that metakaolin addition modifies the optical properties of TiO_2.
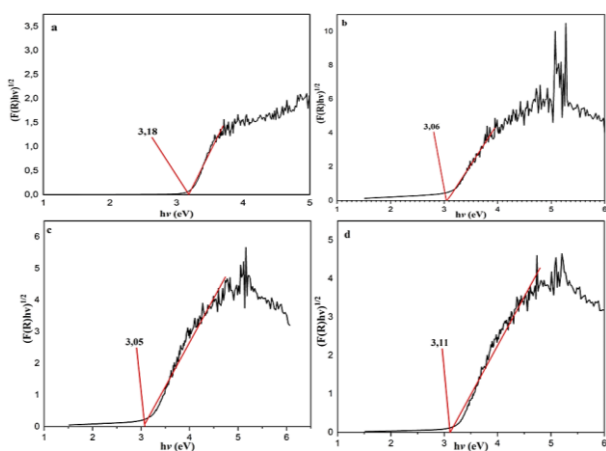
Figure 6. Tauc plot of $[F(R)hv]^{\frac{1}{2}}$ vs E_g for (a) TiO_2, (b) TiO_2-metakaolin 0.5% (w/v), (c) TiO_2-metakaolin 1% (w/v), and (d) TiO_2-metakaolin 1.5% (w/v)

4. Conclusion

The TiO_2-metakaolin composite was successfully synthesized using the sol−gel method. The synthesized TiO_2 exhibited an anatase phase. XRD characterization confirmed that metakaolin and TiO_2-metakaolin composites underwent a phase transition from crystalline to amorphous. FTIR analysis revealed new peak formations and shifts, indicating interactions between TiO_2 and metakaolin. The calculated band gap energies for TiO_2-metakaolin composites with 0.5%, 1%, and 1.5% (w/v) metakaolin were 3.06 eV, 3.05 eV, and 3.11 eV, respectively.

References

[1] Wahyu Febri Ramadhy, Winda Rahmalia, Thamrin Usman, Preparasi dan karakterisasi komposit TiO_2/Metakaolin teraktivasi KOH dalam upaya menurunkan energi celah pita pada anoda TiO_2, *Positron*, 10, 1, (2020), 19−26 https://doi.org/10.26418/positron.v10i1.36703

[2] Eka Pratiwi, Harlia Harlia, Anthoni Batahan Aritonang, Sintesis TiO_2 terdoping Fe^{3+} untuk degradasi rhodamin B secara fotokatalisis dengan bantuan sinar tampak, *Positron*, 10, 1, (2020), 57-63 https://doi.org/10.26418/positron.v10i1.37739

[3] Riri Jonuarti, Triati Dewi Kencana Wungu, Freddy Haryanto, Gel tabir surya berbahan aktif titanium dioksida dengan beberapa variasi perbandingan konsentrasi dalam carbopol (1% b/b), *Prosiding Seminar Nasional Fisika*, 2019

[4] Jong Hyeok Park, Byung-Woo Kim, Jun Hyuk Moon, Dual Functions of Clay Nanoparticles with High Aspect Ratio in Dye-Sensitized Solar Cells, *Electrochemical and Solid-State Letters*, 11, 10, (2008), B171 https://doi.org/10.1149/1.2957601

[5] Dewi Fatmawati, Anthoni B. Aritonang, Sintesis dan Karakterisasi TiO_2-Kaolin Menggunakan Metode Sol Gel, *Jurnal Kimia Khatulistiwa*, 8, 2, (2019), 15-21

[6] Tirta Indah Wulan Sari, Muhsin Muhsin, Hesti Wijayanti, Pengaruh metode aktivasi pada kemampuan kaolin sebagai adsorben besi (Fe) air sumur garuda, *Konversi*, 5, 2, (2016), 20-25 https://dx.doi.org/10.20527/k.v5i2.4768

[7] Ziad Khaled, Alaa Mohsen, AbdelMonem Soltan, Mohamed Kohail, Optimization of kaolin into Metakaolin: Calcination Conditions, mix design and curing temperature to develop alkali activated binder, *Ain Shams Engineering Journal*, 14, 6, (2023), 102142 https://doi.org/10.1016/j.asej.2023.102142

[8] N. Venkatachalam, M. Palanichamy, V. Murugesan, Sol−gel preparation and characterization of alkaline earth metal doped nano TiO_2: Efficient photocatalytic degradation of 4-chlorophenol, *Journal of Molecular Catalysis A: Chemical*, 273, 1, (2007), 177-185 https://doi.org/10.1016/j.molcata.2007.03.077

[9] Susi Lindasari, Kiki Prio Utomo Rudiyansyah, Penentuan Kapasitas Adsorpsi Ion Klorida (Cl^-) pada Pasir Kuarsa Terlapis Mangan Oksida dan Kaolin Teraktivasi HCl, *Jurnal Kimia Khatulistiwa*, 6, 1, (2017), 8-16

[10] Elyta Clarissa, Adhitiyawarman Adhitiyawarman, Anthoni B. Aritonang, Sintesis Co(II)-TiO_2/Kaolin

Sebagai Fotokatalis Antibakteri *Escherichia coli* dengan Bantuan Sinar Tampak, *Indonesian Journal of Pure Applied Chemistry*, 4, 3, (2021), 124-131 https://doi.org/10.26418/indonesian.v4i3.47020

[11] Muthia Elma, *Proses Sol-Gel: Analisis, Fundamental dan Aplikasi*, Lambung Mangkurat University Press, Banjarmasin, 2018,

[12] Dechen Jiang, Jia Tang, Baohong Liu, Pengyuan Yang, Jilie Kong, Ultrathin Alumina Sol-Gel-Derived Films: Allowing Direct Detection of the Liver Fibrosis Markers by Capacitance Measurement, *Analytical Chemistry*, 75, 17, (2003), 4578-4584 https://doi.org/10.1021/ac034046x

[13] Falah A-H. Mutlak, Raied K. Jamal, Ala F. Ahmed, Pulsed Laser Deposition of TiO_2 Nanostructures for Verify the Linear and Non-Linear Optical Characteristics, *Iraqi Journal of Science*, 62, 2, (2021), 517-525 https://doi.org/10.24996/ijs.2021.62.2.18

[14] Aprilina Purbasari, Tjokorde Walmiki Samadhi, Kajian Dehidroksilasi Termal Kaolin menjadi Metakaolin menggunakan Analisis Termogravimetri, *ALCHEMY Jurnal Penelitian Kimia*, 17, 1, (2021), 105-112 https://doi.org/10.20961/alchemy.17.1.47337.105-112

[15] Suzan S. Ibrahim, Ayman A. Hagrass, Tawfik R. Boulos, Samir I. Youssef, Fouad I. El-Hossiny, Mohamed R. Moharam, Metakaolin as an active pozzolan for cement that improves its properties and reduces its pollution hazard, *Journal of Minerals Materials Characterization Engineering*, 6, 1, (2018), 86-104 https://doi.org/10.4236/jmmce.2018.61008

[16] Mónica A. Villaquirán-Caicedo, Studying different silica sources for preparation of alternative waterglass used in preparation of binary geopolymer binders from metakaolin/boiler slag, *Construction and Building Materials*, 227, (2019), 116621 https://doi.org/10.1016/j.conbuildmat.2019.08.002

[17] Yuanyuan Liu, Qian Huang, Liang Zhao, Shaomin Lei, Influence of kaolinite crystallinity and calcination conditions on the pozzolanic activity of metakaolin, *Gospodarka Surowcami Mineralnymi – Mineral Resources Management*, 37, 1, (2021), 39-56 https://doi.org/10.24425/gsm.2021.136295

[18] Shani Sperinck, Metakaolin as a model system for understanding geopolymers, Curtin University, 2012

[19] Zuhua Zhang, Xiao Yao, Huajun Zhu, Sudong Hua, Yue Chen, Activating process of geopolymer source material: Kaolinite, *Journal of Wuhan University of Technology-Materials Science Edition*, 24, (2009), 132-136 https://doi.org/10.1007/s11595-009-1132-6

[20] Indah Permatasari Zuhdi, Analisis Struktur Mikro Kristal pada Serbuk dan Lapisan NiCrAl dengan Elemen Reaktif Si dan Y Menggunakan Metode Scherrer, Fakultas Sains dan Teknologi, UIN Syarif Hidayatullah Jakarta, Jakarta, 2018

[21] Nurfitriyana Nurfitriyana, Najma Annuria Fithri, Fitria, Rini Yanuarti, Analisis interaksi kimia fourier transform infrared (FTIR) tablet gastrorentif ekstrak daun petai (*parkia speciosa hassk*) dengan polimer HPMC-K4M dan kitosan, *ISTA Online Technologi Journal*, 3, 2, (2022), 27-33 https://doi.org/10.62702/ion.v3i2.69

[22] Ruth Ellerbrock, Mathias Stein, Jörg Schaller, Comparing amorphous silica, short-range-ordered silicates and silicic acid species by FTIR, *Scientific Reports*, 12, 1, (2022), 11708 https://doi.org/10.1038/s41598-022-15882-4

[23] Siska Shelvia Deviani, F. Widhi Mahatmanti, Nuni Widiarti, Sintesis dan karakterisasi zeolit dari abu sekam padi menggunakan metode hidrotermal, *Indonesian Journal of Chemical Science*, 7, 1, (2018), 86-93

[24] Rendy Muhamad Iqbal, Erwin Prasetya Toepak, Dyah Ayu Pramoda Wardani, Elda Alyatikah, Stevin Carolius Angga, Luqman Hakim, Study of Microstructure and Optical Properties of Fe_2O_3/TiO_2 Composites as Functional Materials Studi Mikrostruktur dan Sifat Optik Komposit Fe_2O_3/TiO_2 sebagai Material Fungsional, *Jurnal Ilmiah Berkala: Sains dan Terapan Kimia*, 16, 2, (2022), 110-116 https://dx.doi.org/10.20527/jstk.v16i2.12142

[25] Amany W. Ali, E. M. Ezzo, S. A. Hassan, N. G. Mosa, Removal of Methylene Blue from Aqueous Solutions by Anatase doped on Kaolin and Zeolite, *Egyptian Journal of Chemistry*, 66, 12, (2023), 421-430 https://doi.org/10.21608/ejchem.2023.193903.7609

[26] Shofi Nur Aliyah, Dina Kartika Maharani, Pengaruh suhu kalsinasi komposit Zn terhadap karakteristik komposit TiO_2/ZnO, *Unesa Journal of Chemistry*, 10, 1, (2021), 79-84 https://doi.org/10.26740/ujc.v10n1.p79-84

[27] Nidatul Syarifah, Penentuan komposisi TiO_2-N dan lama penyinaran optimum pada fotodegradasi *naphthol blue black* dengan fotokatalis TiO_2-N, Universitas Islam Negeri Maulana Malik Ibrahim, 2022

[28] Salmon Landi, Iran Rocha Segundo, Elisabete Freitas, Mikhail Vasilevskiy, Joaquim Carneiro, Carlos José Tavares, Use and misuse of the Kubelka-Munk function to obtain the band gap energy from diffuse reflectance measurements, *Solid State Communications*, 341, (2022), 114573 https://doi.org/10.1016/j.ssc.2021.114573

[29] Dwi Warono, Syamsudin Ab, Unjuk Kerja Spektrofotometer Untuk Analisa Zat Aktif Ketoprofen, *Jurnal Konversi*, 2, 1, (2013), 57-65

[30] Dessy Ayu Setyawati, Abdul Haris, Sintesis $ZnO-SiO_2$ serta Aplikasinya pada Degradasi Limbah Organik Fenol dan Fotoreduksi Pb(II) secara Simultan, *Jurnal Kimia Sains dan Aplikasi*, 18, 3, (2015), 96-100 https://doi.org/10.14710/jksa.18.3.96-100